BABAR-PUB-12/031
SLAC-PUB-15347

Time-Integrated Luminosity Recorded by the *BABAR* Detector at the PEP-II e^+e^- Collider

J. P. Lees[a], V. Poireau[a], V. Tisserand[a], E. Grauges[b], A. Palano[ab,c], G. Eigen[d], B. Stugu[d], D. N. Brown[e], L. T. Kerth[e], Yu. G. Kolomensky[e], G. Lynch[e], H. Koch[f], T. Schroeder[f], D. J. Asgeirsson[g], C. Hearty[g], T. S. Mattison[g], J. A. McKenna[g], R. Y. So[g], A. Khan[h], V. E. Blinov[i], A. R. Buzykaev[i], V. P. Druzhinin[i], V. B. Golubev[i], E. A. Kravchenko[i], A. P. Onuchin[i], S. I. Serednyakov[i], Yu. I. Skovpen[i], E. P. Solodov[i], K. Yu. Todyshev[i], A. N. Yushkov[i], D. Kirkby[j], A. J. Lankford[j], M. Mandelkern[j], B. Dey[k], J. W. Gary[k], O. Long[k], G. M. Vitug[k], C. Campagnari[l], M. Franco Sevilla[l], T. M. Hong[l], D. Kovalskyi[l], J. D. Richman[l], C. A. West[l], A. M. Eisner[m], W. S. Lockman[m], A. J. Martinez[m], B. A. Schumm[m], A. Seiden[m], D. S. Chao[n], C. H. Cheng[n], B. Echenard[n], K. T. Flood[n], D. G. Hitlin[n], P. Ongmongkolkul[n], F. C. Porter[n], A. Y. Rakitin[n], R. Andreassen[o], Z. Huard[o], B. T. Meadows[o], M. D. Sokoloff[o], L. Sun[o], P. C. Bloom[p], W. T. Ford[p], A. Gaz[p], U. Nauenberg[p], J. G. Smith[p], S. R. Wagner[p], R. Ayad[q,1], W. H. Toki[q], B. Spaan[r], K. R. Schubert[s], R. Schwierz[s], D. Bernard[t], M. Verderi[t], P. J. Clark[u], S. Playfer[u], D. Bettoni[a,v], C. Bozzi[a,v], R. Calabrese[ab,v], G. Cibinetto[ab,v], E. Fioravanti[ab,v], I. Garzia[ab,v], E. Luppi[ab,v], L. Piemontese[a,v], V. Santoro[a,v], R. Baldini-Ferroli[w], A. Calcaterra[w], R. de Sangro[w], G. Finocchiaro[w], P. Patteri[w], I. M. Peruzzi[w,2], M. Piccolo[w], M. Rama[w], A. Zallo[w], R. Contri[ab,x], E. Guido[ab,x], M. Lo Vetere[ab,x], M. R. Monge[ab,x], S. Passaggio[a,x], C. Patrignani[ab,x], E. Robutti[a,x], B. Bhuyan[y], V. Prasad[y], M. Morii[z], A. Adametz[aa], U. Uwer[aa], H. M. Lacker[ab], T. Lueck[ab], P. D. Dauncey[ac], U. Mallik[ad], C. Chen[ae], J. Cochran[ae], W. T. Meyer[ae], S. Prell[ae], A. E. Rubin[ae], A. V. Gritsan[af], N. Arnaud[ag], M. Davier[ag], D. Derkach[ag], G. Grosdidier[ag], F. Le Diberder[ag], A. M. Lutz[ag], B. Malaescu[ag], P. Roudeau[ag], M. H. Schune[ag], A. Stocchi[ag], G. Wormser[ag], D. J. Lange[ah], D. M. Wright[ah], J. P. Burke[ai], J. P. Coleman[ai], J. R. Fry[ai], E. Gabathuler[ai], R. Gamet[ai], D. E. Hutchcroft[ai], D. J. Payne[ai], C. Touramanis[ai], A. J. Bevan[aj], F. Di Lodovico[aj], R. Sacco[aj], M. Sigamani[aj], G. Cowan[ak], D. N. Brown[al], C. L. Davis[al], A. G. Denig[am], M. Fritsch[am], W. Gradl[am], K. Griessinger[am], A. Hafner[am], E. Prencipe[am], R. J. Barlow[an,3], G. D. Lafferty[an], E. Behn[ao], R. Cenci[ao], B. Hamilton[ao], A. Jawahery[ao], D. A. Roberts[ao], C. Dallapiccola[ap], R. Cowan[aq], D. Dujmic[aq], G. Sciolla[aq], R. Cheaib[ar], P. M. Patel[ar,4], S. H. Robertson[ar], P. Biassoni[ab,as], N. Neri[a,as], F. Palombo[ab,as], L. Cremaldi[at], R. Godang[at,5], R. Kroeger[at], P. Sonnek[at], D. J. Summers[at], X. Nguyen[au], M. Simard[au], P. Taras[au], G. De Nardo[ab,av], D. Monorchio[ab,av], G. Onorato[ab,av], C. Sciacca[ab,av], M. Martinelli[aw], G. Raven[aw], C. P. Jessop[ax], J. M. LoSecco[ax], K. Honscheid[ay], R. Kass[ay], J. Brau[az], R. Frey[az], N. B. Sinev[az], D. Strom[az], E. Torrence[az], E. Feltresi[ab,ba], N. Gagliardi[ab,ba], M. Margoni[ab,ba], M. Morandin[a,ba], M. Posocco[a,ba], M. Rotondo[a,ba], G. Simi[a,ba], F. Simonetto[ab,ba], R. Stroili[ab,ba], S. Akar[bb], E. Ben-Haim[bb], M. Bomben[bb], G. R. Bonneaud[bb], H. Briand[bb], G. Calderini[bb], J. Chauveau[bb], O. Hamon[bb], Ph. Leruste[bb], G. Marchiori[bb], J. Ocariz[bb], S. Sitt[bb], M. Biasini[ab,bc], E. Manoni[ab,bc], S. Pacetti[ab,bc], A. Rossi[ab,bc], C. Angelini[ab,bd], G. Batignani[ab,bd], S. Bettarini[ab,bd], M. Carpinelli[ab,bd,6], G. Casarosa[ab,bd], A. Cervelli[ab,bd], F. Forti[ab,bd], M. A. Giorgi[ab,bd], A. Lusiani[ac,bd], B. Oberhof[ab,bd], E. Paoloni[ab,bd], A. Perez[a,bd], G. Rizzo[ab,bd], J. J. Walsh[a,bd], D. Lopes Pegna[be], J. Olsen[be], A. J. S. Smith[be], F. Anulli[a,bf], R. Faccini[ab,bf], F. Ferrarotto[a,bf], F. Ferroni[ab,bf], M. Gaspero[ab,bf], L. Li Gioi[a,bf], M. A. Mazzoni[a,bf], G. Piredda[a,bf], C. Bünger[bg], O. Grünberg[bg], T. Hartmann[bg], T. Leddig[bg], C. Voß[bg], R. Waldi[bg], T. Adye[bh], E. O. Olaiya[bh], F. F. Wilson[bh], S. Emery[bi], G. Hamel de Monchenault[bi], G. Vasseur[bi], Ch. Yèche[bi], D. Aston[bj], D. J. Bard[bj], J. F. Benitez[bj],

[1]Now at the University of Tabuk, Tabuk 71491, Saudi Arabia
[2]Also with Università di Perugia, Dipartimento di Fisica, Perugia, Italy
[3]Now at the University of Huddersfield, Huddersfield HD1 3DH, UK
[4]Deceased
[5]Now at University of South Alabama, Mobile, Alabama 36688, USA
[6]Also with Università di Sassari, Sassari, Italy

Preprint submitted to Elsevier *January 15, 2013*

Published in arXiv:1301.2703.

Work supported by US Department of Energy contract DE-AC02-76SF00515 and HEP.

SLAC National Accelerator Laboratory, Menlo Park, CA 94025

C. Cartaro[bj], M. R. Convery[bj], J. Dorfan[bj], G. P. Dubois-Felsmann[bj], W. Dunwoodie[bj], M. Ebert[bj], R. C. Field[bj], B. G. Fulsom[bj], A. M. Gabareen[bj], M. T. Graham[bj], C. Hast[bj], W. R. Innes[bj], M. H. Kelsey[bj], P. Kim[bj], M. L. Kocian[bj], D. W. G. S. Leith[bj], P. Lewis[bj], D. Lindemann[bj], B. Lindquist[bj], S. Luitz[bj], V. Luth[bj], H. L. Lynch[bj], D. B. MacFarlane[bj], D. R. Muller[bj], H. Neal[bj], S. Nelson[bj], M. Perl[bj], T. Pulliam[bj], B. N. Ratcliff[bj], A. Roodman[bj], A. A. Salnikov[bj], R. H. Schindler[bj], A. Snyder[bj], D. Su[bj], M. K. Sullivan[bj], J. Va'vra[bj], A. P. Wagner[bj], W. F. Wang[bj], W. J. Wisniewski[bj], M. Wittgen[bj], D. H. Wright[bj], H. W. Wulsin[bj], V. Ziegler[bj], W. Park[bk], M. V. Purohit[bk], R. M. White[bk], J. R. Wilson[bk], A. Randle-Conde[bl], S. J. Sekula[bl], M. Bellis[bm], P. R. Burchat[bm], T. S. Miyashita[bm], E. M. T. Puccio[bm], M. S. Alam[bn], J. A. Ernst[bn], R. Gorodeisky[bo], N. Guttman[bo], D. R. Peimer[bo], A. Soffer[bo], S. M. Spanier[bp], J. L. Ritchie[bq], A. M. Ruland[bq], R. F. Schwitters[bq], B. C. Wray[bq], J. M. Izen[br], X. C. Lou[br], F. Bianchi[ab,bs], D. Gamba[ab,bs], S. Zambito[ab,bs], L. Lanceri[ab,bt], L. Vitale[ab,bt], F. Martinez-Vidal[bu], A. Oyanguren[bu], P. Villanueva-Perez[bu], H. Ahmed[bv], J. Albert[bv], Sw. Banerjee[bv], F. U. Bernlochner[bv], H. H. F. Choi[bv], G. J. King[bv], R. Kowalewski[bv], M. J. Lewczuk[bv], I. M. Nugent[bv], J. M. Roney[bv], R. J. Sobie[bv], N. Tasneem[bv], T. J. Gershon[bw], P. F. Harrison[bw], T. E. Latham[bw], H. R. Band[bx], S. Dasu[bx], Y. Pan[bx], R. Prepost[bx], S. L. Wu[bx],

The *BABAR* Collaboration

[a] *Laboratoire d'Annecy-le-Vieux de Physique des Particules (LAPP), Université de Savoie, CNRS/IN2P3, F-74941 Annecy-Le-Vieux, France*
[b] *Universitat de Barcelona, Facultat de Fisica, Departament ECM, E-08028 Barcelona, Spain*
[c] *INFN Sezione di Bari[a]; Dipartimento di Fisica, Università di Bari[b], I-70126 Bari, Italy*
[d] *University of Bergen, Institute of Physics, N-5007 Bergen, Norway*
[e] *Lawrence Berkeley National Laboratory and University of California, Berkeley, California 94720, USA*
[f] *Ruhr Universität Bochum, Institut für Experimentalphysik 1, D-44780 Bochum, Germany*
[g] *University of British Columbia, Vancouver, British Columbia, Canada V6T 1Z1*
[h] *Brunel University, Uxbridge, Middlesex UB8 3PH, United Kingdom*
[i] *Budker Institute of Nuclear Physics SB RAS, Novosibirsk 630090, Russia*
[j] *University of California at Irvine, Irvine, California 92697, USA*
[k] *University of California at Riverside, Riverside, California 92521, USA*
[l] *University of California at Santa Barbara, Santa Barbara, California 93106, USA*
[m] *University of California at Santa Cruz, Institute for Particle Physics, Santa Cruz, California 95064, USA*
[n] *California Institute of Technology, Pasadena, California 91125, USA*
[o] *University of Cincinnati, Cincinnati, Ohio 45221, USA*
[p] *University of Colorado, Boulder, Colorado 80309, USA*
[q] *Colorado State University, Fort Collins, Colorado 80523, USA*
[r] *Technische Universität Dortmund, Fakultät Physik, D-44221 Dortmund, Germany*
[s] *Technische Universität Dresden, Institut für Kern- und Teilchenphysik, D-01062 Dresden, Germany*
[t] *Laboratoire Leprince-Ringuet, Ecole Polytechnique, CNRS/IN2P3, F-91128 Palaiseau, France*
[u] *University of Edinburgh, Edinburgh EH9 3JZ, United Kingdom*
[v] *INFN Sezione di Ferrara[a]; Dipartimento di Fisica, Università di Ferrara[b], I-44100 Ferrara, Italy*
[w] *INFN Laboratori Nazionali di Frascati, I-00044 Frascati, Italy*
[x] *INFN Sezione di Genova[a]; Dipartimento di Fisica, Università di Genova[b], I-16146 Genova, Italy*
[y] *Indian Institute of Technology Guwahati, Guwahati, Assam, 781 039, India*
[z] *Harvard University, Cambridge, Massachusetts 02138, USA*
[aa] *Universität Heidelberg, Physikalisches Institut, Philosophenweg 12, D-69120 Heidelberg, Germany*
[ab] *Humboldt-Universität zu Berlin, Institut für Physik, Newtonstr. 15, D-12489 Berlin, Germany*
[ac] *Imperial College London, London, SW7 2AZ, United Kingdom*
[ad] *University of Iowa, Iowa City, Iowa 52242, USA*
[ae] *Iowa State University, Ames, Iowa 50011-3160, USA*
[af] *Johns Hopkins University, Baltimore, Maryland 21218, USA*
[ag] *Laboratoire de l'Accélérateur Linéaire, IN2P3/CNRS et Université Paris-Sud 11, Centre Scientifique d'Orsay, B. P. 34, F-91898 Orsay Cedex, France*
[ah] *Lawrence Livermore National Laboratory, Livermore, California 94550, USA*
[ai] *University of Liverpool, Liverpool L69 7ZE, United Kingdom*
[aj] *Queen Mary, University of London, London, E1 4NS, United Kingdom*
[ak] *University of London, Royal Holloway and Bedford New College, Egham, Surrey TW20 0EX, United Kingdom*
[al] *University of Louisville, Louisville, Kentucky 40292, USA*
[am] *Johannes Gutenberg-Universität Mainz, Institut für Kernphysik, D-55099 Mainz, Germany*
[an] *University of Manchester, Manchester M13 9PL, United Kingdom*
[ao] *University of Maryland, College Park, Maryland 20742, USA*
[ap] *University of Massachusetts, Amherst, Massachusetts 01003, USA*
[aq] *Massachusetts Institute of Technology, Laboratory for Nuclear Science, Cambridge, Massachusetts 02139, USA*

[ar] McGill University, Montréal, Québec, Canada H3A 2T8
[as] INFN Sezione di Milano[a]; Dipartimento di Fisica, Università di Milano[b], I-20133 Milano, Italy
[at] University of Mississippi, University, Mississippi 38677, USA
[au] Université de Montréal, Physique des Particules, Montréal, Québec, Canada H3C 3J7
[av] INFN Sezione di Napoli[a]; Dipartimento di Scienze Fisiche, Università di Napoli Federico II[b], I-80126 Napoli, Italy
[aw] NIKHEF, National Institute for Nuclear Physics and High Energy Physics, NL-1009 DB Amsterdam, The Netherlands
[ax] University of Notre Dame, Notre Dame, Indiana 46556, USA
[ay] Ohio State University, Columbus, Ohio 43210, USA
[az] University of Oregon, Eugene, Oregon 97403, USA
[ba] INFN Sezione di Padova[a]; Dipartimento di Fisica, Università di Padova[b], I-35131 Padova, Italy
[bb] Laboratoire de Physique Nucléaire et de Hautes Energies, IN2P3/CNRS, Université Pierre et Marie Curie-Paris6, Université Denis Diderot-Paris7, F-75252 Paris, France
[bc] INFN Sezione di Perugia[a]; Dipartimento di Fisica, Università di Perugia[b], I-06100 Perugia, Italy
[bd] INFN Sezione di Pisa[a]; Dipartimento di Fisica, Università di Pisa[b]; Scuola Normale Superiore di Pisa[c], I-56127 Pisa, Italy
[be] Princeton University, Princeton, New Jersey 08544, USA
[bf] INFN Sezione di Roma[a]; Dipartimento di Fisica, Università di Roma La Sapienza[b], I-00185 Roma, Italy
[bg] Universität Rostock, D-18051 Rostock, Germany
[bh] Rutherford Appleton Laboratory, Chilton, Didcot, Oxon, OX11 0QX, United Kingdom
[bi] CEA, Irfu, SPP, Centre de Saclay, F-91191 Gif-sur-Yvette, France
[bj] SLAC National Accelerator Laboratory, Stanford, California 94309 USA
[bk] University of South Carolina, Columbia, South Carolina 29208, USA
[bl] Southern Methodist University, Dallas, Texas 75275, USA
[bm] Stanford University, Stanford, California 94305-4060, USA
[bn] State University of New York, Albany, New York 12222, USA
[bo] Tel Aviv University, School of Physics and Astronomy, Tel Aviv, 69978, Israel
[bp] University of Tennessee, Knoxville, Tennessee 37996, USA
[bq] University of Texas at Austin, Austin, Texas 78712, USA
[br] University of Texas at Dallas, Richardson, Texas 75083, USA
[bs] INFN Sezione di Torino[a]; Dipartimento di Fisica Sperimentale, Università di Torino[b], I-10125 Torino, Italy
[bt] INFN Sezione di Trieste[a]; Dipartimento di Fisica, Università di Trieste[b], I-34127 Trieste, Italy
[bu] IFIC, Universitat de Valencia-CSIC, E-46071 Valencia, Spain
[bv] University of Victoria, Victoria, British Columbia, Canada V8W 3P6
[bw] Department of Physics, University of Warwick, Coventry CV4 7AL, United Kingdom
[bx] University of Wisconsin, Madison, Wisconsin 53706, USA

Abstract

We describe a measurement of the time-integrated luminosity of the data collected by the *BABAR* experiment at the PEP-II asymmetric-energy e^+e^- collider at the $\Upsilon(4S)$, $\Upsilon(3S)$, and $\Upsilon(2S)$ resonances and in a continuum region below each resonance. We measure the time-integrated luminosity by counting $e^+e^- \to e^+e^-$ and (for the $\Upsilon(4S)$ only) $e^+e^- \to \mu^+\mu^-$ candidate events, allowing additional photons in the final state. We use data-corrected simulation to determine the cross sections and reconstruction efficiencies for these processes, as well as the major backgrounds. Due to the large cross sections of $e^+e^- \to e^+e^-$ and $e^+e^- \to \mu^+\mu^-$, the statistical uncertainties of the measurement are substantially smaller than the systematic uncertainties. The dominant systematic uncertainties are due to observed differences between data and simulation, as well as uncertainties on the cross sections. For data collected on the $\Upsilon(3S)$ and $\Upsilon(2S)$ resonances, an additional uncertainty arises due to $\Upsilon \to e^+e^-$ background. For data collected off the Υ resonances, we estimate an additional uncertainty due to the time-dependent efficiency variations, which can affect the short off-resonance runs.

Keywords: *BABAR* integrated luminosity

1. Introduction

The *BABAR* detector operated at the PEP-II asymmetric-energy e^+e^- collider and collected physics data from October 1999 until March 2008. Most of the data were collected at an e^+e^- center-of-mass (CM) energy $\sqrt{s}$ corresponding to the mass of the $\Upsilon(4S)$ resonance [1]. This "on-resonance" $\Upsilon(4S)$ sample contains $(464.8 \pm 2.8) \times 10^6$ $B\overline{B}$ events [2] and is used for the study of B-meson decays, CP violation, and $B^0 - \overline{B}^0$ mixing. Data samples collected at the $\Upsilon(3S)$ and $\Upsilon(2S)$ resonances in 2008 are used for bottomonium studies and for dedicated new-physics searches. For each $\Upsilon(nS)$ resonance ($n = 2, 3, 4$), an "off-resonance" sample was collected for studying continuum $e^+e^- \to q\overline{q}$ events, where q is a u, d, s, or c quark. The off-$\Upsilon(4S)$ sample has a CM energy about 40 MeV below the $\Upsilon(4S)$ peak mass, and the off-$\Upsilon(3S)$ and off-$\Upsilon(2S)$ samples are 30 MeV below the respective peaks. All on- and off-resonance samples are used for charm, τ, two-photon, and QCD physics analyses.

Measurements of production cross sections and branching fractions often depend on knowledge of the time-integrated luminosity $\mathcal{L}$ of the collected data sample. In some cases, the uncertainty on $\mathcal{L}$ is one of the major sources of systematic uncertainty [3]. In addition, in Υ-resonance data analyses, background characteristics or the level of continuum background contamination are often determined from the off-resonance sample. This requires knowledge of the ratio of the integrated luminosities of the on-resonance and off-resonance samples.

In this article, we describe the final analysis of the integrated luminosity of the dataset collected by *BABAR*, incorporating the latest processing and reconstruction of the dataset, improved techniques, and reduced systematic uncertainties relative to previous measurements. The integrated luminosity is measured with Bhabha ($e^+e^- \to e^+e^-$) and dimuon ($e^+e^- \to \mu^+\mu^-$) events. These processes have large, well-known cross sections and simple signatures that are easily identified, thus ensuring high signal-to-background ratios. We use diphoton ($e^+e^- \to \gamma\gamma$) events to estimate some systematic uncertainties and in the determination of the $\Upsilon(2S, 3S) \to e^+e^-$ background contamination. We do not use diphoton events to directly measure the integrated luminosity, due to the significant uncertainty on the cross section for this process, as calculated by available Monte Carlo (MC) generators.

The analysis technique and results are presented here as a resource for future *BABAR* physics publications, as well as future integrated-luminosity measurements at other e^+e^- colliders.

2. Detector and Dataset

The *BABAR* detector is described in detail in Ref. [4], and only a brief description is given here. Charged-particle trajectories are measured with a five-layer silicon vertex tracker and a 40-layer drift chamber (DCH) in a nearly uniform 1.5 T magnetic field. Charged hadron identification is provided by a Cherenkov detector, and photons and electrons are detected in a CsI(Tl) electromagnetic calorimeter (EMC). Muons are identified with resistive plate chambers and limited streamer tubes inserted between the iron layers of the magnetic-field instrumented flux return (IFR).

A two-level trigger system, composed of a hardware ("level-1") stage and a subsequent software ("level-3") stage, is used to decide whether an event is recorded. Both trigger levels use information from the DCH and EMC and employ fast EMC-cluster and track-reconstruction algorithms. IFR information is also used in level 1. Events passing the level-1 and level-3 trigger selections are recorded. After additional prescaling (discussed below), events are processed by the offline reconstruction, where more sophisticated algorithms use information from all detector subsystems. After initial stages of the offline reconstruction, an event selection and classification stage referred to as the offline filter takes place. Classifications of the level-3 trigger and the offline filter are used to preselect events for subsequent data analysis.

The integrated luminosity and its uncertainties are determined separately for several data samples. The $\Upsilon(4S)$ sample is divided into six runs, labeled Run 1 through Run 6. Each run corresponds to a data-taking period with typical shutdowns of no more than a few days or weeks. Shutdown periods between runs are typically several months long. For each run there is also an off-resonance sample, collected during short periods interleaved with on-resonance data-taking periods. The Run-7 sample contains the $\Upsilon(3S)$ and $\Upsilon(2S)$ data, as well as the corresponding off-resonance samples. Run 7 also includes a dataset collected at CM energies above the $\Upsilon(4S)$ resonance, which is not included in this analysis. Table 1 lists the data-taking period and Υ resonance for each run.

To calculate cross sections and detector efficiencies, we make use of simulated MC samples. The `BHWIDE` [5] MC generator is used to simulate Bhabha events, and the `KKMC` [6] generator with the modifications described in Ref. [7] is used for dimuon events.

Table 1: Data-taking period and the resonance corresponding to the PEP-II CM energy $\sqrt{s}$ for each of the *BABAR* runs.

Resonance	Run	Month/Year
$\Upsilon(4S)$	Run 1	10/1999 – 10/2000
	Run 2	02/2001 – 06/2002
	Run 3	12/2002 – 06/2003
	Run 4	09/2003 – 07/2004
	Run 5	04/2005 – 08/2006
	Run 6	01/2007 – 09/2007
$\Upsilon(3S)$	Run 7	12/2007 – 02/2008
$\Upsilon(2S)$	Run 7	02/2008 – 03/2008

We also use KKMC to study possible background from $e^+e^- \to \tau^+\tau^-$ events. The BABAYAGA generator with next-to-leading-order corrections [8] is used to estimate the Bhabha cross section systematic uncertainty. The EvtGen [9] generator is used for studying the background from $\Upsilon(2S)$ and $\Upsilon(3S)$ decays in Run 7. We use the BKQED [10] generator to generate diphoton events. Events produced by these MC generators are passed through a full detector simulation based on Geant4 [11] and are reconstructed and analyzed in the same way as the data.

3. Analysis Method

For Runs 1–6, the integrated luminosity is measured with Bhabha ($e^+e^- \to e^+e^-$) and dimuon ($e^+e^- \to \mu^+\mu^-$) events, which may include any number of radiated photons in the final state. For Run 7, $e^+e^- \to \mu^+\mu^-$ events are not used, due to significant uncertainty associated with the contribution of the $\Upsilon \to \mu^+\mu^-$ background.

For a particular data sample, the integrated luminosity is measured from

$$\mathcal{L} = \frac{N_{\rm cand} - N_{\rm bgd}}{\sigma_{\rm vis}}, \tag{1}$$

where $N_{\rm cand}$ is the number of selected signal candidate events, of which $N_{\rm bgd}$ events are estimated to be background. The visible cross section $\sigma_{\rm vis}$ is given by

$$\sigma_{\rm vis} \equiv \int \frac{d\sigma}{d\Omega}\epsilon(\Omega)\, d\Omega, \tag{2}$$

where $d\sigma/d\Omega$ is the theoretical differential cross section and $\epsilon(\Omega)$ the efficiency for reconstructing and selecting signal events for a given phase-space point Ω. The methods for obtaining each of these quantities are discussed below.

3.1. Event Selection

The event-selection criteria are designed to yield samples of high-purity Bhabha and dimuon events, with two high-momentum charged-particle tracks in the central part of the detector and relatively little energy taken up by radiated photons. We have chosen the selection criteria so that systematic uncertainties arising from data-MC differences of event distributions are kept to a minimum. Electron *vs.* muon identification relies on comparison of the track momentum with the corresponding energy deposited in the EMC. Event selection is performed in two steps: preselection, which takes place at the level-3 trigger and during offline reconstruction, and is described in Section 3.1.1; and final event selection, which is described in Section 3.1.2.

As a basic requirement for tracks at both selection steps, the point of closest approach of the track to the incoming PEP-II beams is required to be less than 1.5 cm in the radial direction (r) and less than 10 cm in the beam direction (z).

3.1.1. Preselection

Tracks used for the level-3 Bhabha event selection must have laboratory-frame polar-angle values between 0.9 rad and 2.5 rad. Most Bhabha events are selected by finding two oppositely charged tracks with CM momenta above 2.0 GeV/c, where at least one of the tracks is associated with an EMC cluster with CM energy of at least 2.5 GeV. The CM momenta, polar angles, and azimuthal angles of the two tracks are required to satisfy $p_1 + p_2 > 7\,{\rm GeV}/c$, $|\theta_1 + \theta_2 - \pi| < 0.5\,{\rm rad}$, and $|\phi_1 - \phi_2 - \pi| < 0.3\,{\rm rad}$. To maintain high efficiency, the level-3 Bhabha selection also accepts events with a single track, provided there is an EMC energy deposition in the expected location, opposite the track in the CM frame. In this case, the requirements on the track momentum, the cluster energy, and the polar and azimuthal angles of the track and cluster are $p_{\rm track} + E_{\rm cluster} > 6\,{\rm GeV}$, $|\theta_{\rm track} + \theta_{\rm cluster} - \pi| < 0.2\,{\rm rad}$, and $|\phi_{\rm track} + \phi_{\rm cluster} - \pi| < 0.3\,{\rm rad}$, where these quantities are evaluated in the CM frame.

Bhabha events are recorded not only for luminosity determination, but also for EMC calibration. The Bhabha cross section increases steeply with decreasing e^+e^- scattering angle. Therefore, a large fraction of events in regions of high cross section is discarded in order to reduce the rate of events handled by the data-acquisition system without significant detrimental impact on calibration. This is achieved by assigning each trigger-selected Bhabha event to one of seven bins according to $\theta^{\rm Lab}_{\rm max}$, the larger of the laboratory-frame polar

angles of the two leptons. For each bin i, only one of every N_i events is logged, where the "prescale factor" N_i increases with $\theta^{\rm Lab}_{\rm max}$. This results in a sawtooth distribution of $\cos\theta^{\rm Lab}_{\rm max}$ that is nonetheless more uniform than the original distribution and more suitable for calibration purposes. The prescale factor applied to each saved event is later used to recreate the initial $|\cos\theta|$ spectrum for use in the luminosity determination.

Dimuon events are passed by the level-3 trigger based on a very loose criterion of a single track with transverse momentum $p_T > 0.6\,\mathrm{GeV}/c$ (a value further reduced for Run 7) or two tracks, each having $p_T > 0.25\,\mathrm{GeV}/c$. This loose selection is possible due to the fact that the $e^+e^- \to \mu^+\mu^-$ cross section is much lower than the $e^+e^- \to e^+e^-$ cross section. At the offline-filter stage, dimuon event selection requires two oppositely charged tracks. The CM momenta of the higher-momentum and lower-momentum tracks must satisfy $p_1 > 4\,\mathrm{GeV}/c$ and $p_2 > 2\,\mathrm{GeV}/c$, respectively; the sum of the CM polar angles of the tracks is required to satisfy $2.8 < \theta_1 + \theta_2 < 3.5\,\mathrm{rad}$; and the sum of the CM energies of the EMC clusters associated with the two tracks must be less than 2 GeV.

The diphoton level-3 trigger selection requires two EMC clusters. During Run 1 data collection, the CM energy of each cluster was required to be at least 0.35 of the PEP-II CM energy $\sqrt{s}$. For Runs 2–7, the requirement was decreased to $0.3\sqrt{s}$. The sums of the polar and azimuthal angles of the clusters must satisfy $|\theta_1+\theta_2-\pi| < \alpha_0$ and $||\phi_1-\phi_2|-\pi| < \alpha_0$ in the CM frame, where $\alpha_0 = 0.5\,\mathrm{rad}$ for Run 1 and 0.1 rad for Runs 2–7. The trigger is rejected if the event has a track with $p_T > 0.25\,\mathrm{GeV}/c$.

To facilitate offline checks of simulated trigger efficiency, a heavily prescaled, unbiased sample of all events satisfying the level-1 trigger is logged. For corresponding checks of the offline-filter stage, a prescaled sample of all logged events is kept regardless of whether any offline-filter selection is satisfied. The use of these "bypass" samples is discussed in Section 3.3.

3.1.2. Final Selection

The Bhabha and dimuon event selections for the luminosity analysis impose additional, tighter final-selection criteria, relying on event properties obtained with the offline reconstruction.

For Bhabha candidates, the CM polar angles of the tracks are required to satisfy $|\cos\theta| < 0.70\,\mathrm{rad}$ for one track and $|\cos\theta| < 0.65\,\mathrm{rad}$ for the other track. We require $P_1 > 0.75$ and $P_2 > 0.50$, where the scaled momentum $P_i \equiv 2p_i/\sqrt{s}$ is twice the ratio of the CM momentum p_i of track i to the PEP-II CM energy $\sqrt{s}$, and the index $i = 1$ ($i = 2$) denotes the track with the higher (lower) CM momentum. The acolinearity angle α, defined as 180° minus the CM angle between the two tracks, is required to satisfy $\alpha < 30°$. We attempt to geometrically associate each track with an EMC cluster and calculate the ratio of the cluster energy to the track momentum in the laboratory frame. Denoting the higher (lower) ratio with $(E/p)_H$ ($(E/p)_L$), we require $(E/p)_H > 0.7$ and $(E/p)_L > 0.4$. If only one track is associated with a cluster, it must satisfy $(E/p) > 0.7$. Events with no track-cluster association are rejected.

For dimuon candidates, we require $|\cos\theta| < 0.70\,\mathrm{rad}$ for one track and $|\cos\theta| < 0.65\,\mathrm{rad}$ for the other track, $P_1 > 0.85$, $P_2 > 0.75$, and $\alpha < 20°$. At least one track must have an associated EMC cluster with CM energy less than 0.5 GeV. If a cluster is associated to the second track, its CM energy is required to be less than 1 GeV.

Diphoton candidates are selected by requiring events with two EMC clusters with energies E_1, E_2 satisfying $2E_1/\sqrt{s} > 0.85$ and $2E_2/\sqrt{s} > 0.75$. The CM polar angles of the clusters must satisfy $|\cos\theta| < 0.7\,\mathrm{rad}$ for one cluster and $|\cos\theta| < 0.65\,\mathrm{rad}$ for the other, and the acolinearity angle must be smaller than 10°. If there are tracks in the event, the track with the largest CM momentum must satisfy $P_1 < 0.5$.

Hadronic events ($e^+e^- \to$ hadrons) are used in the estimation of the $\Upsilon \to e^+e^-$ background. We select such events by requiring at least three tracks and a primary vertex location consistent with the known beamspot. The total energy of tracks and clusters must be greater than $0.3\sqrt{s}$, and the ratio of the second to the zeroth Fox-Wolfram moments [12] is required to be smaller than 0.95. The distance between the primary production vertex of the tracks in the event and the time-averaged beamspot position must be less than 0.5 cm in r and less than 6 cm in z.

Figs. 1 through 4 show examples of the Bhabha and dimuon selection-variable distributions for data and simulation. Although in some cases there are visible differences between the distributions in data and in simulation, the loose selection criteria ensure that these differences have negligible impact on the knowledge of the signal efficiency.

3.2. Background Estimation

3.2.1. Background Sources Common to All Runs

The efficiency for $e^+e^- \to \tau^+\tau^- \to \mu^+\mu^-\nu_\mu\bar{\nu}_\mu\nu_\tau\bar{\nu}_\tau$ events to pass the dimuon selection is determined using MC. We find the fraction of such events in the selected $e^+e^- \to \mu^+\mu^-$ candidate sample to be $(0.0816 \pm 0.0033)\%$. The fraction of Bhabha events in the dimuon

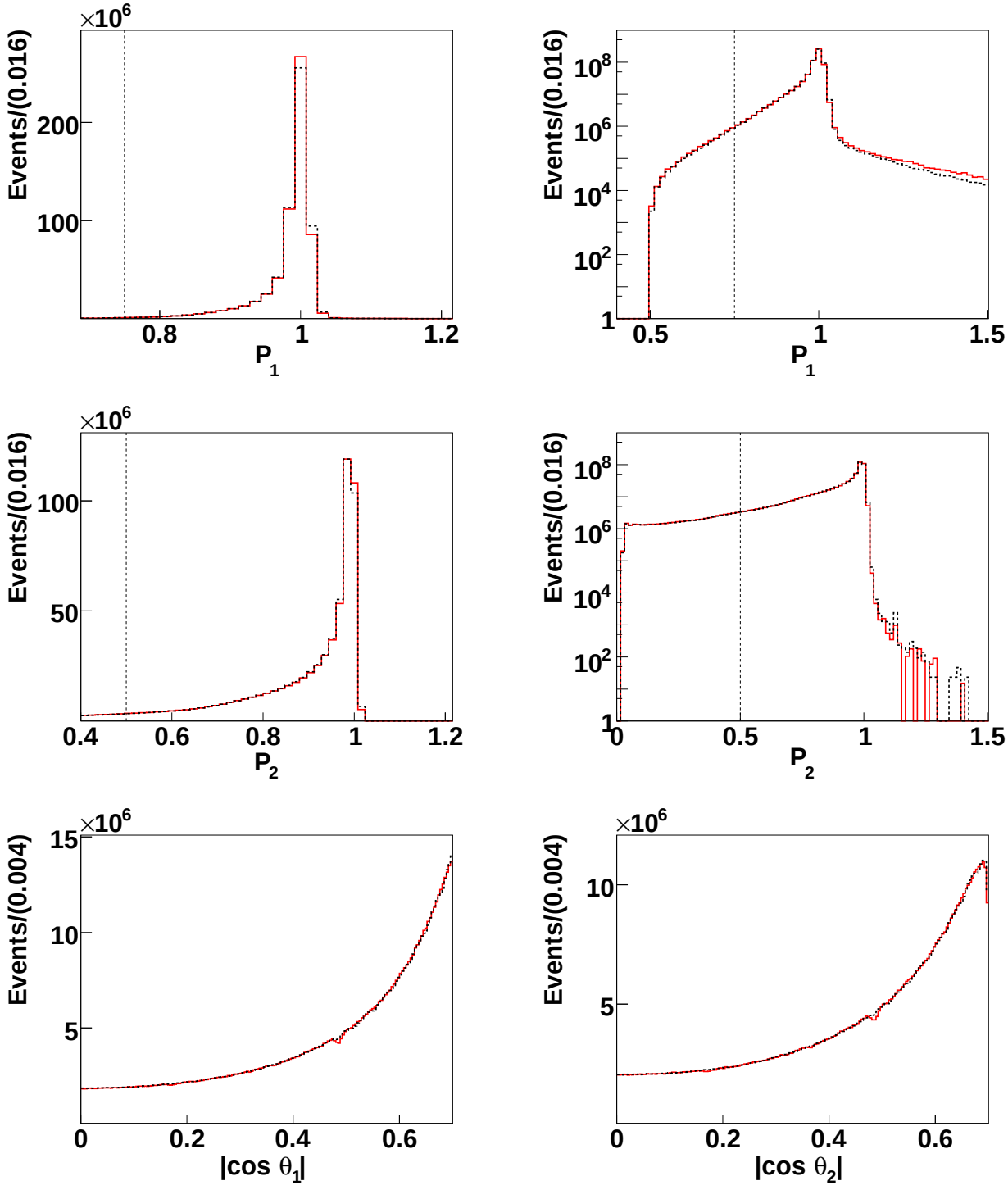

Figure 1: Distributions of the scaled CM momentum $P_i = 2p_i/\sqrt{s}$ and cosine of the CM polar angle θ_i for the higher-momentum ($i = 1$) and lower-momentum ($i = 2$) track in candidate $e^+e^- \to e^+e^-$ events in a fraction of the data (Run 4; solid red histograms) and for simulated $e^+e^- \to e^+e^-$ events (dashed black histograms). The simulation histograms are normalized to the area of the data histograms. The upper two rows of figures show the P_i distributions with linear (left) and log (right) vertical scale. In each scaled-momentum plot, the vertical line shows the minimum value for events that are retained. When plotting each variable, the selection criteria on all other variables are applied. The $|\cos\theta_i|$ ($i = 1, 2$) plots are made with $|\cos\theta_i| < 0.7$.

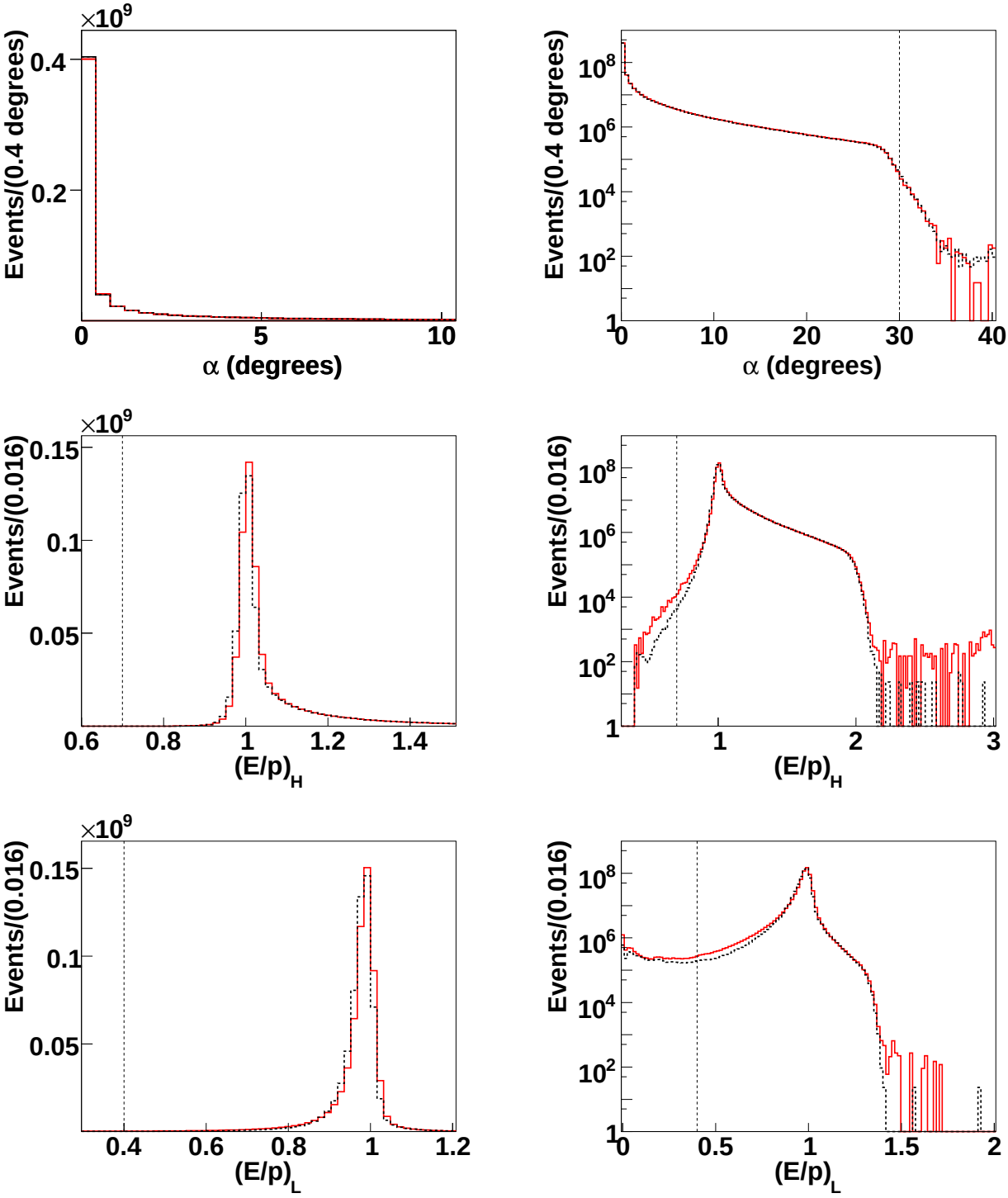

Figure 2: Distributions of the CM acolinearity angle α, and the higher (lower) laboratory-frame energy-to-momentum ratio E/p_H (E/p_L) for $e^+e^- \to e^+e^-$ candidates in a fraction of the data (Run 4; solid red histograms) and for simulated $e^+e^- \to e^+e^-$ events (dashed black histograms). The simulation histograms are normalized to the area of the data histograms. The distributions are shown with linear (left) and log (right) vertical scale. In each E/p plot (log-scale α plot), the vertical line shows the minimum (maximum) value for events that are retained. When plotting each variable, the selection criteria on all other variables are applied.

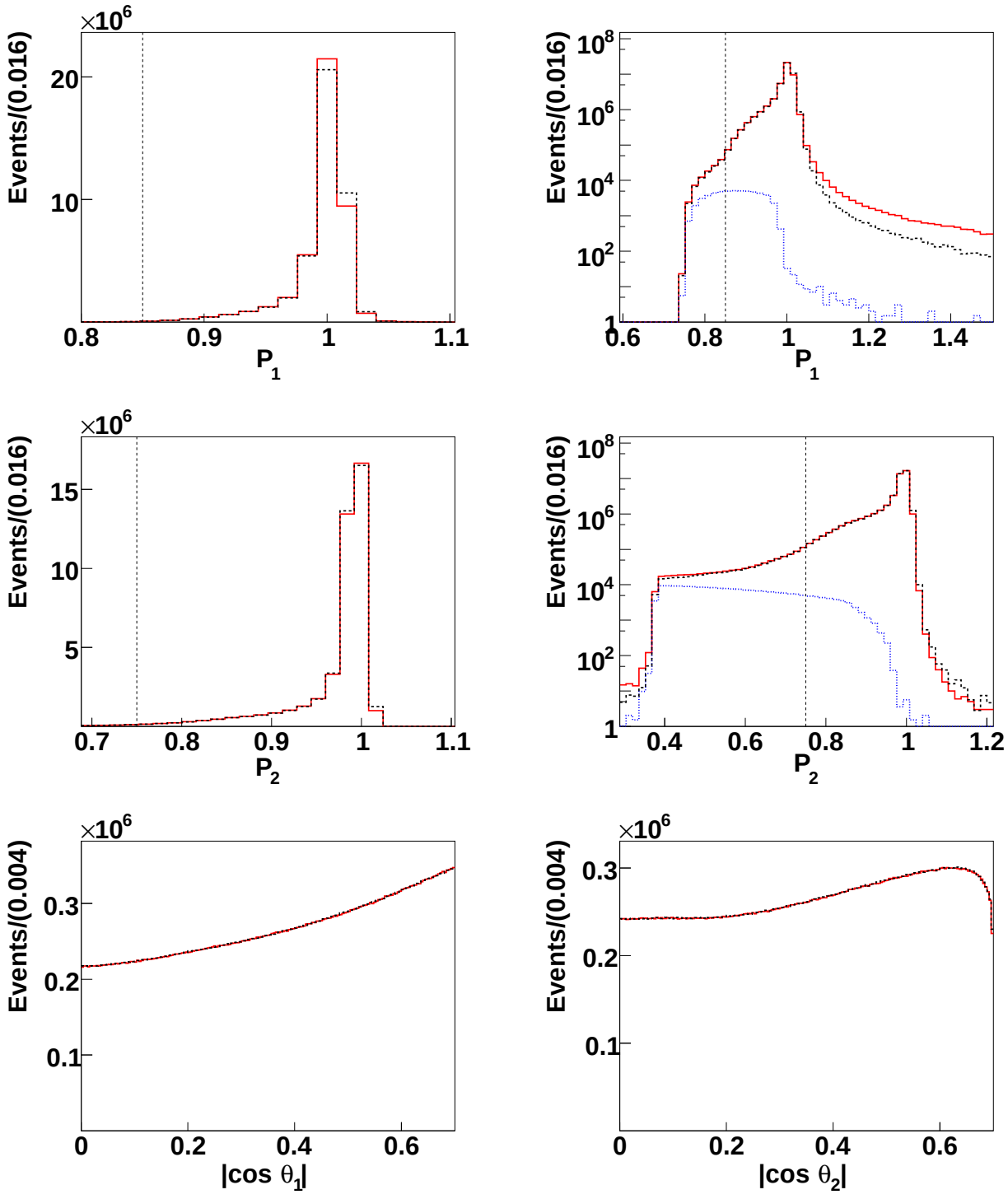

Figure 3: Distributions of the scaled CM momentum $P_i = 2p_i/\sqrt{s}$ and cosine of the CM polar angle θ_i for the higher-momentum ($i = 1$) and lower-momentum ($i = 2$) track in candidate $e^+e^- \to \mu^+\mu^-$ events in a fraction of the data (Run 4; solid red histograms) and for simulated $e^+e^- \to \mu^+\mu^-$ and $e^+e^- \to \tau^+\tau^-$ events (dashed black histograms). In the log-scale plots, the dotted blue histograms show the small contribution of $e^+e^- \to \tau^+\tau^-$ events to the simulation histograms. The simulation histograms are normalized to the area of the data histograms. The upper two rows of figures show the P_i distributions with linear (left) and log (right) vertical scale. In each scaled-momentum plot, the vertical line shows the minimum value for events that are retained. When plotting each variable, the selection criteria on all other variables are applied. The $|\cos\theta_i|$ ($i = 1, 2$) plots are made with $|\cos\theta_i| < 0.7$.

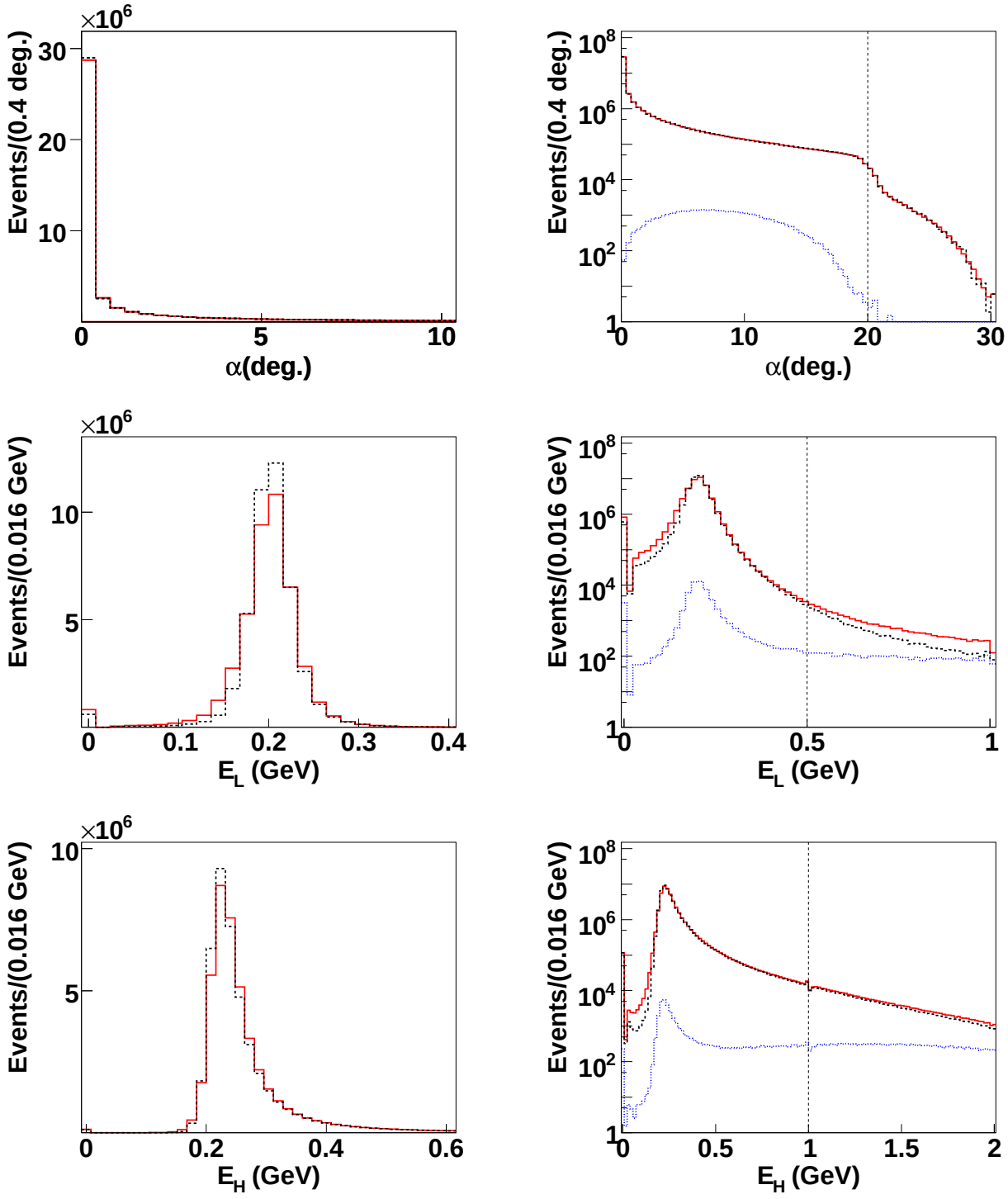

Figure 4: Distributions of the CM acolinearity angle α and of the laboratory-frame energies of the higher-energy (E_H) and lower-energy (E_L) EMC clusters matched to the tracks in candidate $e^+e^- \to \mu^+\mu^-$ events in a fraction of the data (Run 4; solid red histograms) and for simulated $e^+e^- \to \mu^+\mu^-$ and $e^+e^- \to \tau^+\tau^-$ events (dashed black histograms). In each log-scale plot, the dotted blue histogram shows the small contribution of $e^+e^- \to \tau^+\tau^-$ events to the simulation histogram, and the vertical line shows the maximum value for events that are retained. The simulation histograms are normalized to the area of the data histograms. The distributions are shown with linear (left) and log (right) vertical scale. When plotting each variable, the selection criteria on all other variables are applied.

sample is determined in the same way, and is found to be $(0.02 \pm 0.01)\%$. In both cases, the uncertainties are due to MC statistics, and are much larger than those expected due to uncertainties on the efficiency or the cross sections of the various modes.

To estimate the background due to cosmic rays or beam-gas interactions, we select dimuon candidates where the point of closest approach of the tracks to the beamline is between 10 cm and 30 cm of the interaction point in z, and that satisfy all other requirements. From this sample, the level of contamination of cosmic events in the dimuon sample is determined to be $(1.8 \pm 0.7) \times 10^{-5}$, which we take to be negligible.

The background level in the Bhabha sample is much smaller than the values listed above for the dimuon sample, since the visible cross section for $e^+e^- \to e^+e^-$ is an order of magnitude larger than for $e^+e^- \to \mu^+\mu^-$. Therefore, the background in the Bhabha channel is neglected.

3.2.2. Υ Background in Run 7

The on-resonance Run-7 sample contains non-negligible contributions from the decays $\Upsilon(2S) \to e^+e^-$, $\Upsilon(3S) \to e^+e^-$ and, to a smaller extent, from cascade decays such as $\Upsilon(2S) \to \pi^+\pi^-\Upsilon(1S) \to \pi^+\pi^-e^+e^-$ or $\Upsilon(2S) \to \gamma\chi_{bJ}(1P) \to \gamma\gamma\Upsilon(1S) \to \gamma\gamma e^+e^-$. This type of background, which we label as $\Upsilon \to e^+e^-X$, is negligible in the $\Upsilon(4S)$ samples of Runs 1–6. We determine the number of Run-7 $\Upsilon \to e^+e^-X$ events from

$$N_{\Upsilon\to e^+e^-} = N_\Upsilon \mathcal{B}_{\rm vis}(\Upsilon \to e^+e^-X), \tag{3}$$

where N_Υ is the number of $e^+e^- \to \Upsilon$ events produced, and the visible branching fraction

$$\mathcal{B}_{\rm vis}(\Upsilon \to e^+e^-X) = \sum_i \mathcal{B}_i(\Upsilon \to e^+e^-X)\epsilon_i(\Upsilon \to e^+e^-X) \tag{4}$$

accounts for the branching fraction $\mathcal{B}_i(\Upsilon \to e^+e^-X)$ and reconstruction efficiency $\epsilon_i(\Upsilon \to e^+e^-X)$ of each process (indicated by the index i) that contributes to this background. We obtain $\mathcal{B}_{\rm vis}(\Upsilon \to e^+e^-X)$ from simulated events, generated with branching fractions $\mathcal{B}_i(\Upsilon \to e^+e^-X)$ based on the measurements compiled in the Review of Particle Physics [1]. Since $\mathcal{B}(\Upsilon(3S) \to e^+e^-)$ has not been measured, we take its value to be identical to $\mathcal{B}(\Upsilon(3S) \to \mu^+\mu^-)$, relying on lepton universality in electromagnetic interactions.

To determine the number of Υ mesons produced in the $\Upsilon(2S)$ or $\Upsilon(3S)$ on-resonance sample, we count the number of on-resonance hadronic events and subtract the number of off-resonance events scaled by the ratios of luminosities and cross sections between the on- and off-resonance samples. The luminosity ratio is determined from diphoton events. The number of Υ mesons is [2]

$$N_\Upsilon = \left(N_{\rm had} - \kappa N_{\rm had}^{\rm off}\frac{N_{\gamma\gamma}}{N_{\gamma\gamma}^{\rm off}}\right)\frac{1}{\epsilon_{\rm had}}, \tag{5}$$

where $N_{\rm had}$ ($N_{\rm had}^{\rm off}$) is the number of events satisfying the $e^+e^- \to$ hadrons selection criteria in the on-resonance (off-resonance) sample, $N_{\gamma\gamma}$ ($N_{\gamma\gamma}^{\rm off}$) is the number of events satisfying the $e^+e^- \to \gamma\gamma$ selection criteria in the on-resonance (off-resonance) sample, $\epsilon_{\rm had}$ is the reconstruction efficiency for the on-resonance hadronic events, and κ is a correction factor accounting for the small s-dependence of the visible cross sections of the continuum hadronic and $\gamma\gamma$ events.

Using Eq. (3), we determine that $\Upsilon \to e^+e^-$ background constitutes $(1.4 \pm 0.1)\%$ of the events passing the $e^+e^- \to e^+e^-$ selection in the on-resonance $\Upsilon(2S)$ sample and $(0.9 \pm 0.1)\%$ in the $\Upsilon(3S)$ sample. The uncertainties are dominated by the uncertainties on the $\Upsilon \to e^+e^-$ branching fractions. The uncertainty on N_Υ is 0.9%, dominated by the determination of $\epsilon_{\rm had}$, and has a negligible effect on the $N_{\Upsilon\to e^+e^-}$ uncertainty.

In the dimuon channel, $\Upsilon \to \mu^+\mu^-$ events constitute $(21.9 \pm 2.2)\%$ of the selected $e^+e^- \to \mu^+\mu^-$ candidate events for the $\Upsilon(2S)$ sample and $(14.3 \pm 1.4)\%$ for the $\Upsilon(3S)$ sample. Due to the large uncertainty introduced by this background, dimuon events are not used for Run 7, as mentioned above.

3.3. Visible Cross Sections

The visible cross sections $\sigma_{\rm vis}$ (see Eq. (2)) for Bhabha and dimuon events are initially obtained from the MC simulation for each run period and CM energy[7]. We then correct the values of $\sigma_{\rm vis}$ for small data-MC efficiency differences, determined as follows.

We determine the inefficiency of the trigger and offline-filter selection from the fraction of events that fail this selection but satisfy the final selection requirements, using event samples that are allowed to bypass the level-3 trigger and offline filter. From the inefficiency difference between data and MC, we apply run-by-run corrections to $\sigma_{\rm vis}$ of up to 0.3%.

The track-reconstruction inefficiency is measured from the fraction of Bhabha events in which only one

[7] The MC generators are not valid in some parts of phase space, in particular for small-angle Bhabha scattering, which is excluded by the analysis selection criteria. Therefore, the simulation can be used to evaluate the visible cross section, but not the full cross section and efficiency separately.

track is found. To minimize the non-Bhabha events in this sample, one of the tracks must satisfy tight selection criteria: $0.95 < P < 1.05$, $0.9 < (E/p) < 1.1$, and $|\cos\theta| < 0.70$ rad. A second track is not found in 0.2% of these events. The identification of these one-track events as $e^+e^- \to e^+e^-$ is justified by the observation that the highest-energy EMC cluster, other than the cluster associated with the track, has CM acolinearity with respect to the track of no more than about 10° (some acolinearity is expected, since the missed track bends in the magnetic field), and that the ratio between the energy of this cluster to the track momentum peaks at 1. From the data-MC inefficiency difference, we apply run-dependent corrections to $\sigma_{\rm vis}$ in the range 0.14%-0.27%.

Table 2 shows the corrected visible cross sections for the different PEP-II CM energies. For Runs 1–6, we observe a run-to-run variation of ±0.21% (±0.7%) in the value of $\sigma_{\rm vis}$ for the Bhabha (dimuon) channel.

Table 2: Visible cross section $\sigma_{\rm vis}$ (see Eq. (2)) for the different data-taking periods categorized according to the center-of-mass energy $\sqrt{s}$, which was equal to ("On") or just below ("Off") the masses of the Υ resonances. Results for the $\Upsilon(4S)$ samples are luminosity-averaged over Runs 1–6. The uncertainties are systematic and are described in Section 4.

Sample	$\sigma_{\rm vis}$ (nb)	
	$e^+e^- \to e^+e^-$	$e^+e^- \to \mu^+\mu^-$
On $\Upsilon(4S)$	6.169 ± 0.041	0.4294 ± 0.0023
Off $\Upsilon(4S)$	6.232 ± 0.044	0.4333 ± 0.0025
On $\Upsilon(3S)$	6.461 ± 0.037	0.4488 ± 0.0028
Off $\Upsilon(3S)$	6.508 ± 0.056	0.4501 ± 0.0040
On $\Upsilon(2S)$	6.933 ± 0.042	0.4802 ± 0.0030
Off $\Upsilon(2S)$	6.866 ± 0.051	0.4721 ± 0.0036

4. Systematic Uncertainties

Table 3 summarizes the systematic uncertainties, which are described in detail below.

For the selection criteria used in this analysis, we find that the cross section reported by BHWIDE is consistent with that of the BABAYAGA [13] generator to within the statistical uncertainty of the comparison, 0.06%. We add this uncertainty in quadrature to the BABAYAGA theoretical uncertainty of 0.20% [13] to obtain the total uncertainty of 0.21%. The uncertainty on the dimuon cross sections is taken to be 0.44%, based on Ref. [7].

From the data-MC comparisons described in Section 3.3, we estimate an uncertainty of 0.13% (0.20%) for the track-reconstruction efficiency for Runs 1–6 (Run 7), corresponding to approximately half the largest correction within these data samples. An uncertainty of 0.1% is estimated for the trigger and offline-filter efficiency correction by rounding up the largest of the run-dependent statistical uncertainties of this correction. To account for differences between the distributions of data and MC events in the variables used for event selection, we vary the selection requirements over wide ranges throughout the tails of the signal-event distributions, and repeat the full analysis for each variation. For each run, the largest resulting change in $\mathcal{L}$ is taken to be the associated uncertainty, with values ranging between 0.40% and 0.60%.

The luminosity and systematic uncertainties are evaluated for the entire period of data collection for each particular run. Use of subsamples within a run may introduce time-dependent variations in efficiency that are not accounted for in the analysis. In particular, off-resonance data are collected at relatively rare intervals, and could therefore be subject to such time-dependent effects. Therefore, we estimate an additional systematic uncertainty for the off-resonance luminosity, accounting for tracking-related and EMC-related time variation studied using the on-resonance samples. The on-resonance data sample for each run is divided into at least ten subsamples with luminosities of about 1 to 2 fb^{-1} each. In each subsample i, we calculate the ratio $x_i = \mathcal{L}_i^{ee}/\mathcal{L}_i^{\mu\mu}$ of the luminosity values obtained with Bhabha and dimuon events. We use the spread in the x_i values, after subtraction of the estimated statistical component of the spread, to estimate the off-resonance luminosity uncertainty associated with the time variation of any EMC-related effects. Similarly, we use the spread of the ratios $\mathcal{L}_i^{ee}/\mathcal{L}_i^{\gamma\gamma}$ of the luminosity values obtained with Bhabha and diphoton events to estimate the uncertainty due to the time variation of tracking-related effects. Finally, these two uncertainties are added in quadrature.

The uncertainties on the background subtraction, described in Section 3.2, are propagated to the final uncertainty on $\mathcal{L}$. For Run 7, we estimate an additional uncertainty of 0.2% on the signal reconstruction efficiency, arising from the uncertainty on the laboratory-to-CM boost associated with changing the PEP-II energy from the $\Upsilon(4S)$ to the $\Upsilon(3S)$ and $\Upsilon(2S)$.

Systematic uncertainties from the different sources are added in quadrature, separately for each channel ($e^+e^- \to e^+e^-$, $e^+e^- \to \mu^+\mu^-$), run, and on/off-resonance data-taking period. When combining results in Section 5, we take into account the following correlations between systematic uncertainties. The uncertainties on the track-reconstruction efficiency and on the

Table 3: Relative systematic uncertainties on the measured integrated luminosity.

Source	Relative uncertainty on $\mathcal{L}$ (%)
Theoretical cross section	0.26 (e^+e^-), 0.44 ($\mu^+\mu^-$)
Track-reconstruction efficiency	0.13 (Runs 1–6), 0.20 (Run 7)
Trigger & offline-filter efficiency	0.10
Data-MC differences	0.40–0.60
Time dependence	0.16–0.46 (Off-resonance)
Background subtraction	0.02 (Runs 1–6), 0.10 ($\Upsilon(3S)$), 0.15 ($\Upsilon(2S)$)
Boost uncertainty	0.2 (Run 7)

trigger and offline-filter efficiency are positively correlated between the two channels. Uncertainties in the theoretical cross section, background subtraction, trigger and offline-filter efficiencies, and selection-criteria variation are positively correlated for the different runs, as well as for the on-resonance and off-resonance periods.

5. Results

Table 4 lists the integrated luminosity results for the on- and off-resonance samples for each run. The results for Runs 1–6 are averaged over the $\mu^+\mu^-$ and e^+e^- channels, accounting for correlated uncertainties. The results obtained with the two modes are compatible and have similar overall uncertainties, with the $\mu^+\mu^-$ uncertainties being somewhat smaller. (As noted in Section 3, the Run-7 luminosity is obtained with e^+e^- events only.) The ratios between the on-resonance and off-resonance integrated luminosities are also given. Table 5 shows a run-by-run breakdown of the results for the $\Upsilon(4S)$ periods.

6. Acknowledgements

We are grateful for the extraordinary contributions of our PEP-II colleagues in achieving the excellent luminosity and machine conditions that have made this work possible. The success of this project also relies critically on the expertise and dedication of the computing organizations that support *BABAR*. The collaborating institutions wish to thank SLAC for its support and the kind hospitality extended to them. This work is supported by the US Department of Energy and National Science Foundation, the Natural Sciences and Engineering Research Council (Canada), the Commissariat à l'Energie Atomique and Institut National de Physique Nucléaire et de Physique des Particules (France), the Bundesministerium für Bildung und Forschung and Deutsche Forschungsgemeinschaft (Germany), the Istituto Nazionale di Fisica Nucleare (Italy), the Foundation for Fundamental Research on Matter (The Netherlands), the Research Council of Norway, the Ministry of Education and Science of the Russian Federation, Ministerio de Ciencia e Innovación (Spain), and the Science and Technology Facilities Council (United Kingdom). Individuals have received support from the Marie-Curie IEF program (European Union) and the A. P. Sloan Foundation (USA).

References

[1] Particle Data Group, J. Beringer *et al.*, Phys. Rev. D86, 010001 (2012).
[2] G. D. McGregor, SLAC-R-912 (2008) (arXiv:0812.1954 [hep-ex]).
[3] For example, *BABAR* Collaboration, B. Aubert *et al.*, Phys. Rev. Lett. 100 (2008) 011801; *BABAR* Collaboration, B. Aubert *et al.*, Nucl. Phys. Proc. Suppl. 189 (2009) 193.
[4] *BABAR* Collaboration, B. Aubert *et al.*, Nucl. Instrum. Meth. A 479 (2002) 1.
[5] S. Jadach, W. Placzek and B. F. L. Ward, Phys. Lett. B 390 (1997) 298.
[6] S. Jadach, B. F. L. Ward and Z. Was, Comput. Phys. Commun. 30 (2000) 260.
[7] S. Banerjee, B. Pietrzyk, J. M. Roney and Z. Was, Phys. Rev. D 77 (2008) 054012.
[8] G. Balossini *et al.*, Nucl. Phys. B 758 (2006) 227.
[9] D. J. Lange, Nucl. Instrum. Meth. A 462 (2001) 152.
[10] F. A. Berends and R. Kleiss, Nucl. Phys. B 186 (1981) 22; W. Placzek, S. Jadach, M. Melles, B. F. L. Ward and S. A. Yost, arXiv:hep-ph/9903381 (1999).
[11] Geant4 Collaboration, S. Agostinelli *et al.*, Nucl. Instrum. Meth. A 506 (2003) 250.
[12] G. C. Fox, S. Wolfram, Phys. Rev. Lett. 41 (1978) 1581.
[13] G. Balossini, C. M. Carloni Calame, G. Montagna, O. Nicrosini and F. Piccinini, Nucl. Phys. Proc. Suppl. 162 (2006) 59.
[14] W. Beenakker, F. A. Berends and S. C. van der Marck, Nucl. Phys. B 349 (1991) 323.

Table 4: The integrated luminosities of the on-resonance ($\mathcal{L}_{\rm on}$) and off-resonance ($\mathcal{L}_{\rm off}$) data samples recorded at and just below the Υ resonances, and the ratio between the on- and off-resonance integrated luminosities. The first uncertainties are statistical and the second uncertainties are systematic.

Resonance	$\mathcal{L}_{\rm on}$ (fb^{-1})	$\mathcal{L}_{\rm off}$ (fb^{-1})	$\mathcal{L}_{\rm on}/\mathcal{L}_{\rm off}$
$\Upsilon(4S)$	$424.18 \pm 0.04 \pm 1.82$	$43.92 \pm 0.01 \pm 0.19$	$9.658 \pm 0.003 \pm 0.007$
$\Upsilon(3S)$	$27.96 \pm 0.03 \pm 0.16$	$2.623 \pm 0.008 \pm 0.017$	$10.66 \pm 0.03 \pm 0.03$
$\Upsilon(2S)$	$13.60 \pm 0.02 \pm 0.09$	$1.419 \pm 0.006 \pm 0.011$	$9.58 \pm 0.04 \pm 0.04$

Table 5: The on-resonance ($\mathcal{L}_{\rm on}$) and off-resonance ($\mathcal{L}_{\rm off}$) integrated luminosities of the individual $\Upsilon(4S)$ runs, and the ratio between the on- and off-resonance integrated luminosities. The first uncertainties are statistical and the second uncertainties are systematic.

Run	$\mathcal{L}_{\rm on}$ (fb^{-1})	$\mathcal{L}_{\rm off}$ (fb^{-1})	$\mathcal{L}_{\rm on}/\mathcal{L}_{\rm off}$
1	$20.37 \pm 0.01 \pm 0.09$	$2.564 \pm 0.002 \pm 0.014$	$7.946 \pm 0.006 \pm 0.027$
2	$61.32 \pm 0.01 \pm 0.26$	$6.868 \pm 0.004 \pm 0.034$	$8.928 \pm 0.006 \pm 0.023$
3	$32.28 \pm 0.01 \pm 0.13$	$2.443 \pm 0.003 \pm 0.012$	$13.213 \pm 0.015 \pm 0.037$
4	$99.58 \pm 0.02 \pm 0.41$	$10.016 \pm 0.007 \pm 0.043$	$9.943 \pm 0.007 \pm 0.012$
5	$132.33 \pm 0.02 \pm 0.59$	$14.278 \pm 0.008 \pm 0.066$	$9.268 \pm 0.005 \pm 0.012$
6	$78.31 \pm 0.02 \pm 0.35$	$7.752 \pm 0.006 \pm 0.036$	$10.102 \pm 0.008 \pm 0.013$